In vivo observation of lidocaine-encapsulated Polymyxin/glycol nanoparticles wound dressing for the treatment and care of abdominal pain incision in intensive care unit

Zhenfei Pan
First People's Hospital of Wenling
Jinqiang Zhu
First People's Hospital of Wenling
Yi Mao
First People's Hospital of Wenling
Zhenzhen Jiang
First People's Hospital of Wenling
Wei Wu
First People's Hospital of Wenling
Yamei Shao
First People's Hospital of Wenling
Lili Chen (lili.chen55@yahoo.com)
First People's Hospital of Wenling https://orcid.org/0000-0002-5242-0942

Original Research

Keywords: lidocaine chloride, Polymyxin (PMN)/Glycol (GLY), Wound healing, Abdominal Pain management, In vivo mouse model

Posted Date: February 11th, 2021

DOI: https://doi.org/10.21203/rs.3.rs-207852/v1

Version of Record: A version of this preprint was published at Journal of Polymers and the Environment on April 15th, 2021. See the published version at https://doi.org/10.1007/s10924-021-02093-7.

Abstract

The developments of lidocaine chloride loaded nanoparticles are encouraging biomaterials, which could be used for wound healing applications for abdominal pain management. The current work presents the composition of wound dressings based on lidocaine chloride (LCH) (anesthetic drug)-loaded Polymyxin (PMN)/Glycol (GLY). The LCH nanocomposite (LCH@PMN/GLY) were fabricated by the LCH oxide solutions within the PMN/GLY matrix. The influences of different experimental limitations on PMN/GLY nanoparticles formations were examined. The PMN/GLY and LCH@PMN/GLY nanoparticle sizes were evaluated by high resolution-scanning electron microscopy (HR-SEM). Additionally, the antibacterial efficacy of PMN/GLY and LCH@PMN/GLY was developed for gram-positive and negative microorganisms. Moreover, we examined *in vivo* healing of skin wounds formed in mouse models over 20 days. In contrast to the untreated wounds, rapid healing was perceived in the LCH@PMN/GLY-treated wound with less damage. These findings indicate that LCH@PMN/GLY-based bandaging materials could be a potential innovative biomaterial for tissue repair and implantation and nursing care for wound healing applications for abdominal pain incision in intensive care unit (ICU) management in an animal model.

1. Introduction

Infections cause problems in the field of wound management because they form exudates and limit wound improvement, leading to the use of inappropriate sponges. Microorganisms are the main cause of infections [1–4]. The most common infection-producing microorganisms are *E. coli* and Klebsiella, which are gram-negative bacteria. On entering the human body, these microorganisms quickly establish colonies. These organisms can penetrate the cell nanocomposite in the body, and enter the actual fractions of tissues and cells, leading to internal infections. Therefore, wound dressings are required to prevent these bacterial infections [5–8].

Postoperative adhesion (POA) is a comprehensive inflection of various abnormal tissue hyperplasias, characterized by proliferated fibrous tissues sticking to the nearby normal organs [9–11]. The adhesion bands can take diversified phenotypes ranging from a thin layer of fibrous films between the adjacent tissues to a mixture of fibrous tissues, blood vessels, and nerves [12–14]. Depending on distinct positions and levels of the adhesion, POA may be accompanied with acute complications or be “silent” for several years. These complications, such as chronic pain, dysfunction of adjacent organs, and intestinal obstruction, can reduce the life quality of patients or even become life threatening [15–17]. Even non-sterilized wounds can increase the incidence of infections, leading to exudate formation around the edges. This leads to the use of various polymers, nanocomposite, and cryogels to improve wound dressings. However, previous studies have shown that these materials have limitations such as moisture entry, air passage, biocompatibility, environmental safety, and higher toxicity [18–20]. The use of biological polymers, such as keratin, gelatin, heparin, hyaluronic acid, cellulose, chitosan, chitin, and alginic acid, for wound dressings is less economical. The use of Polymyxin B (PMN) and Glycol (GLY) nanocomposite formulations to heal serious burn and bone tissue injuries has been reported earlier [21–

23]. The PMN/GLY nanocomposite is easy to deliver, biocompatible, and biodegradable; additionally, it has low toxicity. The nanocomposite compositions and thin films have antibacterial properties with low damage clearness capacity and high stability [24–26].

Furthermore, several research groups have shown the incorporation of montmorillonite clay into PMN/GLY nanocomposites for wound bandaging applications. Anisha et al. developed chitosan hyaluronic acid-coated LCH nanoparticles (LCH) to counter drug-resistant bacteria for wound bandage applications [27–31]. Chitin-covered LCH have also demonstrated promising wound management. Additionally, the nanocomposite based on alginate-coated PMN/GLY with LCH have shown promising fluid absorption capabilities and antimicrobial properties [32–34].

In the present study, we aimed to develop wound bandages based on PMN/GLY and LCH. The first step involved the fabrication of LCH inside the PMN/GLY matrix (LCH@PMN/GLY) by PMN/GLY as important agents. Further, the surface of LCH was modified by adding PMN/GLY (LCH@PMN/GLY). The GLY, PMN, and LCH@PMN/GLY were subsequently covered with cotton fabrics to generate the final composites. The wound bandaging studies were performed with the GLY, PMN and LCH@PMN/GLY composites utilizing antimicrobials *in vitro* and *in vivo* animal models.

2. Experimental Section

2.1. Materials

LCH oxide solutions, Polymyxin B (Mn = 80 000), Glycol (GLY) (medium molecular weight) and 3-(4,5-dimethylthiazol-2-yl)-2,5-diphenyltetrazolium bromide (MTT) were acquired from TCI, China. Luria broth and agar-agar were purchased from J&D, China. Bacterials strains of *S. aureus* and *E. coli* were obtained from our institutions. Cotton fabrics were obtained from local suppliers. All chemicals and reagents were used without further purification.

2.2. Fabrication of LCH@PMN/GLY nanocomposite scaffolds

A polymer solution of PMN/GLY was prepared by mixing 10% w/v PMN and 20% w/v GLY in hexafluoroisopropanol (HFIP)/dichloromethane (DCM) solvent system for 6–12 h. For LCH loaded PMN/GLY, a 25% v/v 30 mM LCH solution was added to the polymer solution; whereas for control samples nanoparticle solution was replaced with similar amount of distilled water. The resulting nanocomposites were collected for characterisation and cell culture studies, respectively [35–37].

2.3. Characterization of PMN/GLY and LCH@PMN/GLY

The morphological properties were studied by scanning electron microscopy (HR-SEM) using a TECNAI-SEM (USA) instrument. In the HR-SEM analysis, one drop of the prepared PMN/GLY sample was placed on a carbon-coated SEM grid at room temperature. Fifty-five readings of the SEM images were recorded to evaluate the ratio of the size and distribution. Dynamic light scattering (DLS, Beckmann-Coulter, Delsa-

Nano) was used to analyze the particle size, size distribution, and polydispersity index of the nanoparticles [38–40].

2.4. Synthesis of PMN/GLY and LCH@PMN/GLY nanocomposites for bandaging

A nanocomposite of PMN/GLY and LCH@PMN/GLY for bandaging was fabricated by the DIP coating method. Briefly, cotton fabric was dished into the PMN/GLY and LCH@PMN/GLY solution, removed, and dehydrated at ~ 60°C for 24 h. The moisture contents of the PMN/GLY and LCH@PMN/GLY matrix were examined. The samples were accurately weighed and subsequently dehydrated in a hot-oven for 5 h. The dehydrated fabrics of cotton were desiccated for 24 h to remove moisture and weighed again. The moisture contents of the PMN/GLY and LCH@PMN/GLY were calculated using a previously reported protocol [41–44].

2.5. *In vitro* biodegradation and swelling studies

To study the biodegradation of the LCH, PMN/GLY and LCH@PMN/GLY nanocomposite, 0.5 g (W_i) of LCH, PMN/GLY and LCH@PMN/GLY nanocomposite were immersed in 50 mL of phosphate-buffered saline (PBS) and incubated at 37°C for 7 days. Concurrently, a blank determination was performed in PBS on the same sample without the nanocomposite. After a period of 1, 4, and 7 days, the samples were washed several times with deionized water and dried in the oven at 40 ± 1°C for 24 h.

The swelling ratio of the LCH, PMN/GLY and LCH@PMN/GLY nanocomposite was measured according to the described methods [45–47]. To measure the water sorption potential of the LCH, PMN/GLY and LCH@PMN/GLY nanocomposite, 0.1 g of dried powder of LCH, PMN/GLY and LCH@PMN/GLY nanocomposite were immersed in 30 mL of PBS with the desired pH at room temperature for 16 h to achieve maximum swelling equilibrium, then removed and gently pressed between filter papers and weighed.

2.6. Antibacterial properties of PMN/GLY and LCH@PMN/GLY

The antibacterial properties of the synthesized PMN/GLY and LCH@PMN/GLY were examined using *E. coli* and *S. aureus* bacteria. The microorganism colony volumes were 10^4 percent/mL. The nanocomposite samples were added to the culture dishes and maintained at 37°C for 24 h. The marked phases of the flexible microbes were quantified in the same manner as the microbes with the saline and agar plates. Bacterial growth rates were examined using statistical models. The cell viability in the synthesized nanocomposite was evaluated using the NIH-3T3 fibroblasts by Alamar Blue assay. The sterilized samples were placed in 96-well plates with the same fluency as the fibroblasts. The cells were marked for three different days. Cell viability was measured at 520 nm using a microplate reader. The experiments were repeated three times [48–51].

2.7. Animal experiments of the wound bandaging model

The animal experiments were performed according to the guidelines of the [2]Department of Cardiology, Fuwai Central Cardiovascular Hospital, Henan Provincial People's Hospital, Zhengzhou 45000, China. Sprague-Dawley rats aged 4 weeks and weighing 200 g were used. The rats were anesthetized by injecting ketamine (30 mg/kg) and xylazine (4 mg/kg). The upper phase of the rat's hair was detached and the specific sites were marked by skin hygienic through the soul. A 1.5 cm-wide skin damage was created in the dorsum of the rats using operating scissors and tongs. The wounds were covered with the baseline damage and used as the negative control (Group I), nanocomposite -loaded bandaging (Group II), PMN/GLY (Group III), and LCH@PMN/GLY (Group IV). The extent of wound closure was analyzed by drawing the wound boundary at the end of 0, 4, 8 and 16 days. The wounds closure was expressed in mm^2. The wounds area was calculated using previously reported methods [52–54].

2.8. Statistical analysis

All inventory data are uttered as the mean ± standard deviations. Significant changes among groups were examined using one-way examination of modification, and changes for separate groups were dogged using Student's t tests. The outcomes were observed as a significant differences when $p < 0.05$.

3. Results And Discussion

3.1. Fabrication and characterization

By employing an easy and effective method to fabricate LCH, the current study aimed at using PMN/GLY as a stabilizing agents as well as a nanocomposite system for the encapsulation of LCH. To avoid the clusters collisions and their growing into macro nanoparticle, the hydroxy fragments of PMN/GLY interact with the LCH and aid in steadying them and preventing their agglomeration and further proliferation. The graphical representation of the generation and anchoring of LCH within a PMN/GLY nanocomposite matrix is depicted in Fig. 1. Morphology analysis of PMN/GLY and LCH@PMN/GLY was carried out by observing the nanocomposite using SEM. The SEM micrographs of PMN/GLY and LCH@PMN/GLY shown in Fig. 2A **and B** reveal isotropic and randomly oriented nanocomposite with a seemingly smooth morphology. The SEM images correspond to the DLS analysis results. The time-dependent difference in DLS analysis shows the particle size and diameters of the nanoparticles. The role of PMN/GLY is to stabilize the nanoparticle formation and provide the base matrix for the nanocomposites.

3.2. Fabrication of PMN/GLY and LCH@PMN/GLY nanocomposites for bandaging

Cotton fabrics were used as permeable, sustainable substrates for preparing PMN/GLY and LCH@PMN/GLY nanocomposites. It has been preferred over other kinds of cotton because of its intrinsic properties, natural abundance, comfort, hydrophilicity, and higher heat conduction. The cotton fabrics were dished into the PMN/GLY and LCH@PMN/GLY solutions and dehydrated at 55 ^{o}C. The interactions amid the cotton fabrics and colloidal solutions resulted in physicochemical absorption of the gels on the

surface of the cotton. The range of the cottons varied from 0.9 to 3.1 % dips of coating enhanced from 1 to 4. It was witnessed that the bandaging showed a little improved flexibility with increase in the nanocomposite content.

3.3. LCH@PMN/GLY surface morphology

The morphology of the nanocomposite was observed by SEM. The SEM images in Fig. 2 show the uncovered fabric form as well as the smooth surface of the fabricated LCH@PMN/GLY. The additions of GLY/PMN-to-PMN/GLY persuades significant differences in the superficial morphology of the covered fabrics with an intricate shell-like system on the surfaces. PMN/GLY enhances the rigidity and flexibility of the bandaging, though the tacky nature facilitates relaxed elimination from the wounded sites. After the releases of LCH, the morphological observations showed larger variations than those prior to release. The SEM images show the effectiveness of LCH on the wounded sites. After the release of LCH, the bandage surface became rigid, rough, and flexible [55–57].

3.4. Mechanical Properties

The mechanical properties of nanocomposite and nanocomposite are critical for successful dressing applications in order to confirm the integrity of the nanocomposite [58–60]. The mechanical properties for pure materials (LCH@PMN/GLY), as prepared PMN/GLY and LCH@PMN/GLY are shown in Fig. 3A. The addition of LCH to the LCH@PMN/GLY had a variable influence on tensile strength and the overall elongation. The PMN/GLY and LCH@PMN/GLY exhibited a tensile strength of 2.2 ± 0.6 and 2.9 ± 0.4 MPa, respectively, which was sufficient for tissue covering the wound. (Fig. 3B). The increased compressive strength means that the samples are more fragmented. These findings have shown that the composites PMN/GLY has strong surface strength suited for therapeutic use [61–63]. The break elongation values represent the LCH and PMN/GLY bandage versatility. Pure LCH, PMN/GLY and LCH@PMN/GLY, the as-prepared PMN/GLY exhibited an elongation in the range from 20–50% at the fracture points (Fig. 3C). Figure 3 also shows that the tensile strength increased with an increase in LCH concentration. The results of the tensile modulus (Fig. 3D) was consistent with the stress test. Overall, PMN/GLY demonstrated higher tensile modulus and elongation than LCH, PMN/GLY and LCH@PMN/GLY, however it exhibited lower maximum strength. Therefore, flexibility would be an important consideration for the application of LCH@PMN/GLY nanocomposites for various types of wound surface [35–38].

3.5. Biodegradation and swelling studies

Nanocomposites have become the subject of improvement for use in many applications [64–66]. The percentage weight loss (Fig. 4A) revealed limited degradation of the LCH@PMN/GLY bandages. All the as-fabricated bandages showed a degradation of 24 to 27% (1 day), 39 to 48% (4 days) and 75 to 84% (7 days) after immersion in PBS medium, respectively. The presence of LCH reduced the degradation rate in the composite bands. The interaction of LCH, PMN/GLY and LCH@PMN/GLY bandages can be due to this. However the as-manufactured bandage has been *in vitro* deteriorated although its features and shape have remained unaltered even after the 7th day. After 1, 4 and 7 days of incubation in PBS

medium, swellings of the PMN/GLY and LCH@PMN/GLY dressings were examined (Fig. 4B). Figure 4B suggested that LCH@PMN/GLY exhibited higher swelling capacity compared to pure PMN/GLY nanocomposite [50–52]. Furthermore, even after LCH were introduced, the nGel and LCH@PMN/GLY bands displayed similar swelling behaviour. The existence of LCH nanoparticles of different dimensions, morphology and surface charges will lead to an improvement in the swelling capacity of LCH@PMN/GLY. Furthermore, nanoparticles forming LCH may cause the LCH@PMN/GLY to expand, widening pores and the open spaces in LCH@PMN/GLY, thus absorbing more water [33].

3.6. Antibacterial and cell viability analyses

The antibacterial properties of the fabricated PMN/GLY and LCH@PMN/GLY dressings were investigated using *S. aureus* (gram-positive microbe) and *E. coli* (gram-negative microbe), and the results are shown in Fig. 5A **and B**. In our previous studies, the LCH@PMN/GLY dressings exhibited higher antibacterial activity with both microbes compared to LCH@PMN/GLY. The bacterial property of LCH@PMN/GLY was reduced by the presence of free LCH@PMN/GLY.

The outcomes of cell viability established that LCH (positive control) and PMN/GLY (control) did not demonstrate any harm on days 1, 3, and 7 in development with NIH-3T3 fibroblasts (Fig. 6A **and B**). The synthesized LCH@PMN/GLY dressings showed ~ 75% viability after day 1 of culture, which further increased up to ~ 93 % after 3 and 7 days of development. The reduced cell viability on day 1 was due to the presence of free PMN/GLY with the NIH3T3 fibroblasts. After day 1, the remaining viable fibroblasts multiplied, consequently improving the viability.

3.7. *In vivo* examination of LCH

The results of the *in vivo* investigation of the PMN/GLY and LCH@PMN/GLY are shown in Fig. 7. The PMN/GLY and LCH@PMN/GLY dressings displayed outstanding wound healing properties after 0, 4, 8 and 16 days, compared to saline treatment (Fig. 7A). The reduction in wound damage in mouse models at different periods (0, 4, 8, 16 and 20 days) can be seen in the Fig. 7. The treatment with fabric control displayed ~ 50 % wound reduction after day 16, while coating with nanocomposite bandaging resulted in 70 % reduction. The LCH@PMN/GLY -treated wound attained 80 % closure on day 16. LCH@PMN/GLY treated mice had almost complete wound closure after day 20. This improved rate of wound closure was attributed to the rapid healing properties of the LCH released from the bandaging in the presence of GLY and PMN (Fig. 7B). The LCH released from the nanocomposites slowly changed the physiological conditions and interacted with specific wound sites. Further, LCH has been gambled to decrease the period for fibroblast to enter wounds. It also has excellent anti-inflammatory properties, which may enhance the re-epithelialization rate [67].

3.8. Histological evaluation

Histological study is a powerful tool for observing improvement in cure and tissue regeneration. The histological based on a specified on the healing potential of damaged mouse tissue caused by the effect on the PMN/GLY and LCH@PMN/GLY (Fig. 8) by hematoxyl and eosin (H&E). After 0, 4, 8, 16 and 20 days, the LCH@PMN/GLY displayed excellent healing as compared to the naked wound. Figure 8 shows that compact keratinocytes in the epidermis are indicated for PMN/GLY and LCH@PMN/GLY wounds relative to the bare wound in histological parts. Furthermore, LCH@PMN/GLY also increased the healing rate of GLY/PMN-coated wounds as shown in the histological micrograms. LCH nanoparticles have biocompatible and anticoagulant properties, making it an excellent candidate for wound cure, as shown in the study *in vitro* and *in vivo*. In comparison, a segment light microscopy quantitated absolute new subcutaneous tissue growth. The degree of wound closure was macroscopically calculated (Fig. 8). Therefore, *in vivo* study of Sprague-Dawley rats confirmed the increased wound healing ability of the as-fabricated LCH@PMN/GLY. The results (Fig. 8) suggested that the LCH@PMN/GLY nanocomposite treatment promotes significant healing through the migration of fibroblasts and appropriate development of epithelial cells, and the restoration of blood flow via training of new blood vessels [68]. In our effort to introduce a tissue treating method, we have developed LCH@PMN/GLY bandage material based on PMN/GLY conjugated with LCH, which was first tested for tissue regeneration care management, to the best of knowledge

4. Conclusion

Our study aimed at developing novel wound bandages by covering double nanocomposite loaded with LCH on the surface of cotton fabrics. Herein, cotton acts as a supporting layer for the nanocomposite. Well-dispersed LCH are generated with the stabilizing effect of PMN/GLY as the nanocomposite medium. The nanocomposite thus formed had a size in the series of ~ 10–50 nm. Together PMN/GLY and LCH@PMN/GLY nanocomposite bandages showed significant antibacterial properties even at low absorptions. A slow rate of releases were detected for the nanocomposites bandages with ~ 2 μg/cm^2 of LCH leaking out in 48 h. These low attentions of LCH are very nontoxic for the human body. The LCH@PMN/GLY bandaging displayed 100 % closure of full width wound by day 20, which may be because the occurrence of PMN/GLY quickens in the medium, therefore assisting wounds closure. The wound bandages might be effortlessly exposed off from the wounds sites without affecting the tissues. The results of these investigations suggest that LCH@PMN/GLY could be a promising wounds care management composition having effective damage and scar prevention.

Declarations

Acknowledgements

None

Authors' contributions

Zhenfei Pan, Jinqiang Zhu, and Yi Mao assisted with NP synthesis and characterization; Zhenzhen Jiang, and Yamei Shao assisted with molecular and biochemical analysis; Wei Wu assisted with data curation, formal analysis, and validation; Lili Chen assisted with supervised the research.

Funding

None

Ethics approval and consent to participate

All animal experiments were approved by the Ethics Committee of the Emergency Intensive Care Unit, Wenling First People's Hospital, Wenling 317500, China in accordance with the guidelines on animal care and use (File No: 2019-10).

Consent for publication

Not applicable.

Competing interests

The authors declare that they have no competing interests.

References

1. Mehrabi T, Mesgar AS, Mohammadi Z (2020) Bioactive Glasses: A Promising Therapeutic Ion Release Strategy for Enhancing Wound Healing, ACS Biomater. Sci Eng 6:5399–5430. https://doi.org/10.1021/acsbiomaterials.0c00528
2. Xiao M, Gao L, Chandrasekaran AR, Zhao J, Tang Q, Qu Z, Wang F, Li L, Yang Y, Zhang X, Wan Y, Pei H (2019) Bio-functional G-molecular hydrogels for accelerated wound healing. Mater Sci Eng C 105:110067. https://doi.org/https://doi.org/10.1016/j.msec.2019.110067
3. Yu B, He C, Wang W, Ren Y, Yang J, Guo S, Zheng Y, Shi X (2020) Asymmetric Wettable Composite Wound Dressing Prepared by Electrospinning with Bioinspired Micropatterning Enhances Diabetic Wound Healing, ACS Appl. Bio Mater 3:5383–5394. https://doi.org/10.1021/acsabm.0c00695
4. Son B, Lee S, Kim H, Kang H, Kim J, Youn H, Nam SY, Youn B (2019) Low dose radiation attenuates inflammation and promotes wound healing in a mouse burn model. J Dermatol Sci 96:81–89. https://doi.org/https://doi.org/10.1016/j.jdermsci.2019.10.004
5. Schmidt CA, Murillo R, Heinzmann B, Laufer S, Wray V, Merfort I (2011) Structural and Conformational Analysis of Proanthocyanidins from Parapiptadenia rigida and Their Wound-Healing Properties. J Nat Prod 74:1427–1436. https://doi.org/10.1021/np200158g
6. Bakshi MS (2017) Nanotoxicity in Systemic Circulation and Wound Healing. Chem Res Toxicol 30:1253–1274. https://doi.org/10.1021/acs.chemrestox.7b00068

7. Zhang X, Yin Z, Guo Y, Huang H, Zhou J, Wang L, Bai J, Fan Z (2020) A facile and large-scale synthesis of a PVA/chitosan/collagen hydrogel for wound healing. New J Chem 44:20776–20784. https://doi.org/10.1039/D0NJ04016A
8. Chen Z, Hu Y, Li J, Zhang C, Gao F, Ma X, Zhang J, Fu C, Geng F (2019) A feasible biocompatible hydrogel film embedding Periplaneta americana extract for acute wound healing. Int J Pharm 571:118707. https://doi.org/https://doi.org/10.1016/j.ijpharm.2019.118707
9. Nielsen ES, Garnås E, Jensen KJ, Hansen LH, Olsen PS, Ritz C, Krych L, Nielsen DS (2018) Lacto-fermented sauerkraut improves symptoms in IBS patients independent of product pasteurisation – a pilot study. Food Funct 9:5323–5335. https://doi.org/10.1039/C8FO00968F
10. Zhang S, Hou J, Yuan Q, Xin P, Cheng H, Gu Z, Wu J (2020) Arginine derivatives assist dopamine-hyaluronic acid hybrid hydrogels to have enhanced antioxidant activity for wound healing. Chem Eng J 392:123775
11. Wang M, Hu G, Tian Y, Zhang Z, Song R (2016) Influence of wine-processing on the pharmacokinetics of anthraquinone aglycones and glycosides from rhubarb in hyperlipidemic hamsters. RSC Adv 6:24871–24879. https://doi.org/10.1039/C5RA27273D
12. Mori da Cunha MGMC, Arts B, Hympanova L, Rynkevic R, Mackova K, Bosman AW, Dankers PYW, Deprest J (2020) Functional supramolecular bioactivated electrospun mesh improves tissue ingrowth in experimental abdominal wall reconstruction in rats. Acta Biomater 106:82–91. https://doi.org/https://doi.org/10.1016/j.actbio.2020.01.041
13. Li J, Feng X, Liu B, Yu Y, Sun L, Liu T, Wang Y, Ding J, Chen X (2017) Polymer materials for prevention of postoperative adhesion. Acta Biomater 61:21–40. https://doi.org/https://doi.org/10.1016/j.actbio.2017.08.002
14. Hernández-Gascón B, Peña E, Melero H, Pascual G, Doblaré M, Ginebra MP, Bellón JM, Calvo B (2011) Mechanical behaviour of synthetic surgical meshes: Finite element simulation of the herniated abdominal wall. Acta Biomater 7:3905–3913. https://doi.org/https://doi.org/10.1016/j.actbio.2011.06.033
15. Peters MF, Choy AL, Pin C, Leishman DJ, Moisan A, Ewart L, Guzzie-Peck PJ, Sura R, Keller DA, Scott CW, Kolaja KL (2020) Developing in vitro assays to transform gastrointestinal safety assessment: potential for microphysiological systems. Lab Chip 20:1177–1190. https://doi.org/10.1039/C9LC01107B
16. Xian C, Gu Z, Liu G, Wu J (2020) Whole wheat flour coating with antioxidant property accelerates tissue remodeling for enhanced wound healing. Chinese Chem Lett 31:1612–1615
17. Bobde Y, Biswas S, Ghosh B (2020) Current trends in the development of HPMA-based block copolymeric nanoparticles for their application in drug delivery. Eur Polym J 139:110018. https://doi.org/https://doi.org/10.1016/j.eurpolymj.2020.110018
18. Hamdan S, Pastar I, Drakulich S, Dikici E, Tomic-Canic M, Deo S, Daunert S (2017) Nanotechnology-Driven Therapeutic Interventions in Wound Healing: Potential Uses and Applications. ACS Cent Sci 3:163–175. https://doi.org/10.1021/acscentsci.6b00371

19. Zhong Z, Huang Y, Hu Q, He W, Duan B, Yan X, Yang Z, Liang W, Liu Z, Peng Z, Wang Y, Zhang L, Ye Q (2019) Elucidation of molecular pathways responsible for the accelerated wound healing induced by a novel fibrous chitin dressing. Biomater Sci 7:5247–5257. https://doi.org/10.1039/C9BM00404A
20. Sekhon UDS, Sen Gupta A (2018) Platelets and Platelet-Inspired Biomaterials Technologies in Wound Healing Applications, ACS Biomater. Sci Eng 4:1176–1192. https://doi.org/10.1021/acsbiomaterials.7b00013
21. Wu R, Du D, Bo Y, Zhang M, Zhang L, Yan Y (2019) Hsp90α promotes the migration of iPSCs-derived keratinocyte to accelerate deep second-degree burn wound healing in mice. Biochem Biophys Res Commun 520:145–151. https://doi.org/https://doi.org/10.1016/j.bbrc.2019.09.120
22. Thakur R, Chattopadhyay P, Mukherjee AK, The wound healing potential of a pro-angiogenic peptide purified from Indian Russell's viper (Daboia russelii) venom, Toxicon. 165 (2019) 78–82. https://doi.org/https://doi.org/10.1016/j.toxicon.2019.04.009
23. Ghuman S, Ncube B, Finnie JF, McGaw LJ, Mfotie Njoya E, Coopoosamy RM, Van Staden J (2019) Antioxidant, anti-inflammatory and wound healing properties of medicinal plant extracts used to treat wounds and dermatological disorders. South African J Bot 126:232–240. https://doi.org/https://doi.org/10.1016/j.sajb.2019.07.013
24. Preman NK, Prabhu SPES,A, Shaikh SB, Barki VC,RR, Bhandary YP, Rekha PD, Johnson RP (2020) Bioresponsive supramolecular hydrogels for hemostasis, infection control and accelerated dermal wound healing. J Mater Chem B 8:8585–8598. https://doi.org/10.1039/D0TB01468K
25. Liu H, Wang C, Li C, Qin Y, Wang Z, Yang F, Li Z, Wang J (2018) A functional chitosan-based hydrogel as a wound dressing and drug delivery system in the treatment of wound healing. RSC Adv 8:7533–7549. https://doi.org/10.1039/C7RA13510F
26. Chen M, Tian J, Liu Y, Cao H, Li R, Wang J, Wu J, Zhang Q (2019) Dynamic covalent constructed self-healing hydrogel for sequential delivery of antibacterial agent and growth factor in wound healing. Chem Eng J 373:413–424. https://doi.org/https://doi.org/10.1016/j.cej.2019.05.043
27. Muhamed I, Sproul EP, Ligler FS, Brown AC (2019) Fibrin Nanoparticles Coupled with Keratinocyte Growth Factor Enhance the Dermal Wound-Healing Rate. ACS Appl Mater Interfaces 11:3771–3780. https://doi.org/10.1021/acsami.8b21056
28. Sharifi S, Hajipour MJ, Gould L, Mahmoudi M (2020) Nanomedicine in Healing Chronic Wounds: Opportunities and Challenges. Mol Pharm. https://doi.org/10.1021/acs.molpharmaceut.0c00346
29. Sun L, Huang Y, Bian Z, Petrosino J, Fan Z, Wang Y, Park KH, Yue T, Schmidt M, Galster S, Ma J, Zhu H, Zhang M (2016) Sundew-Inspired Adhesive Hydrogels Combined with Adipose-Derived Stem Cells for Wound Healing. ACS Appl Mater Interfaces 8:2423–2434. https://doi.org/10.1021/acsami.5b11811
30. Kim SH, Park J-W (2019) IDH2 deficiency impairs cutaneous wound healing via ROS-dependent apoptosis, Biochim. Biophys. Acta - Mol. Basis Dis 1865:165523. https://doi.org/https://doi.org/10.1016/j.bbadis.2019.07.017

31. Jahan I, George E, Saxena N, Sen S (2019) Silver-Nanoparticle-Entrapped Soft GelMA Gels as Prospective Scaffolds for Wound Healing. ACS Appl Bio Mater 2:1802–1814. https://doi.org/10.1021/acsabm.8b00663
32. Simoska O, Duay J, Stevenson KJ (2020) Electrochemical Detection of Multianalyte Biomarkers in Wound Healing Efficacy. ACS Sensors 5:3547–3557. https://doi.org/10.1021/acssensors.0c01697
33. Shah SA, Sohail M, Khan S, Minhas MU, de Matas M, Sikstone V, Hussain Z, Abbasi M, Kousar M (2019) Biopolymer-based biomaterials for accelerated diabetic wound healing: A critical review. Int J Biol Macromol 139:975–993. https://doi.org/https://doi.org/10.1016/j.ijbiomac.2019.08.007
34. Schmidt CA, Murillo R, Bruhn T, Bringmann G, Goettert M, Heinzmann B, Brecht V, Laufer SA, Merfort I (2010) Catechin Derivatives from Parapiptadenia rigida with in Vitro Wound-Healing Properties. J Nat Prod 73:2035–2041. https://doi.org/10.1021/np100523s
35. Deal HE, Brown AC, Daniele MA (2020) Microphysiological systems for the modeling of wound healing and evaluation of pro-healing therapies. J Mater Chem B 8:7062–7075. https://doi.org/10.1039/D0TB00544D
36. Sponchioni M, Capasso Palmiero U, Moscatelli D (2019) Thermo-responsive polymers: Applications of smart materials in drug delivery and tissue engineering. Mater Sci Eng C 102:589–605. https://doi.org/https://doi.org/10.1016/j.msec.2019.04.069
37. Shen T, Dai K, Yu Y, Wang J, Liu C (2020) Sulfated chitosan rescues dysfunctional macrophages and accelerates wound healing in diabetic mice. Acta Biomater. https://doi.org/https://doi.org/10.1016/j.actbio.2020.09.035
38. Bao Z, Gu Z, Xu J, Zhao M, Liu G, Wu J (2020) Acid-responsive composite hydrogel platform with space-controllable stiffness and calcium supply for enhanced bone regeneration. Chem Eng J 396:125353
39. Guo B, Ma PX (2014) Synthetic biodegradable functional polymers for tissue engineering: a brief review. Sci China Chem 57:490–500. https://doi.org/10.1007/s11426-014-5086-y
40. Kalashnikova I, Das S, Seal S (2015) Nanomaterials for wound healing: scope and advancement. Nanomedicine (Lond) 10:2593–2612. https://doi.org/10.2217/NNM.15.82
41. Memic A, Abudula T, Mohammed HS, Joshi Navare K, Colombani T, Bencherif SA (2019) Latest Progress in Electrospun Nanofibers for Wound Healing Applications, ACS Appl. Bio Mater 2:952–969. https://doi.org/10.1021/acsabm.8b00637
42. Kuhlmann M, Wigger-Alberti W, Mackensen Yv, Ebbinghaus M, Williams R, Krause-Kyora F, Wolber R (2019) Wound healing characteristics of a novel wound healing ointment in an abrasive wound model: A randomised, intra-individual clinical investigation. Wound Med 24:24–32. https://doi.org/https://doi.org/10.1016/j.wndm.2019.02.002
43. Kong X, Fu J, Shao K, Wang L, Lan X, Shi J (2019) Biomimetic hydrogel for rapid and scar-free healing of skin wounds inspired by the healing process of oral mucosa. Acta Biomater 100:255–269. https://doi.org/https://doi.org/10.1016/j.actbio.2019.10.011

44. Cheng C-C, Yang X-J, Fan W-L, Lee A-W, Lai J-Y (2020) Cytosine-Functionalized Supramolecular Polymer-Mediated Cellular Behavior and Wound Healing. Biomacromolecules 21:3857–3866. https://doi.org/10.1021/acs.biomac.0c00938
45. Jayaramudu T, Ko H-U, Kim HC, Kim JW, Li Y, Kim J (2017) Transparent and semi-interpenetrating network P(vinyl alcohol)- P(Acrylic acid) hydrogels: pH responsive and electroactive application. Int J Smart Nano Mater 8:80–94. https://doi.org/10.1080/19475411.2017.1335247
46. Pandit AH, Mazumdar N, Imtiyaz K, Rizvi MMA, Ahmad S (2019) Periodate-Modified Gum Arabic Cross-linked PVA Hydrogels: A Promising Approach toward Photoprotection and Sustained Delivery of Folic Acid. ACS Omega 4:16026–16036. https://doi.org/10.1021/acsomega.9b02137
47. Nugraheni A, Purnawati D, Rohmatillah A, Mahardika D, Kusumaatmaja A, Swelling of PVA/Chitosan/TiO2 Nanofibers Membrane in Different PH, Mater Sci Forum 990 (2020) 220–224. https://doi.org/10.4028/www.scientific.net/MSF.990.220
48. Mohamed Kasim MS, Sundar S, Rengan R (2018) Synthesis and structure of new binuclear ruthenium(II) arene benzil bis(benzoylhydrazone) complexes: Investigation on antiproliferative activity and apoptosis induction. Inorganic Chemistry Frontiers 5:585–596. doi:10.1039/c7qi00761b
49. Mohamed Subarkhan MK, Ren L, Xie B, Chen C, Wang Y, Wang H (2019) Novel tetranuclear ruthenium(II) arene complexes showing potent cytotoxic and antimetastatic activity as well as low toxicity in vivo. European Journal of Medicinal Chemistry 179:246–256. doi:https://doi.org/10.1016/j.ejmech.2019.06.061
50. Sathiya Kamatchi T, Mohamed Subarkhan MK, Ramesh R, Wang H, Małecki JG (2020) Investigation into antiproliferative activity and apoptosis mechanism of new arene Ru(ii) carbazole-based hydrazone complexes. Dalton Transactions 49:11385–11395. doi:10.1039/D0DT01476A
51. Mohamed Subarkhan MK, Ramesh R, Liu Y, Synthesis and molecular structure of arene ruthenium(II) benzhydrazone complexes: Impact of substitution at the chelating ligand and arene moiety on antiproliferative activity, New Journal of Chemistry 40 (2016). doi:10.1039/c6nj01936f
52. Niu Y, Yang T, Ke R, Wang C (2019) Preparation and characterization of pH-responsive sodium alginate/humic acid/konjac hydrogel for L-ascorbic acid controlled release. Mater Express 9:563–569
53. Huang J, Chen L, Yuan Q, Gu Z, Wu J (2019) Tofu-Based hybrid hydrogels with antioxidant and low immunogenicity activity for enhanced wound healing. J Biomed Nanotechnol 15:1371–1383
54. Bao Z, Xian C, Yuan Q, Liu G, Wu J (2019) Natural Polymer-Based Hydrogels with Enhanced Mechanical Performances: Preparation, Structure, and Property. Adv Healthc Mater 8:1900670
55. Chouhan D, Dey N, Bhardwaj N, Mandal BB (2019) Emerging and innovative approaches for wound healing and skin regeneration: Current status and advances. Biomaterials 216:119267. https://doi.org/https://doi.org/10.1016/j.biomaterials.2019.119267
56. Li W, Wang Y, Qi Y, Zhong D, Xie T, Yao K, Yang S, Zhou M (2020) Cupriferous Silver Peroxysulfite Superpyramids as a Universal and Long-Lasting Agent to Eradicate Multidrug-Resistant Bacteria and Promote Wound Healing. ACS Appl Bio Mater. https://doi.org/10.1021/acsabm.0c00889

57. Rameshbabu AP, Datta S, Bankoti K, Subramani E, Chaudhury K, Lalzawmliana V, Nandi SK, Dhara S (2018) Polycaprolactone nanofibers functionalized with placental derived extracellular matrix for stimulating wound healing activity. J Mater Chem B 6:6767–6780. https://doi.org/10.1039/C8TB01373J
58. Sun X, Wang X, Zhao Z, Chen J, Li C, Zhao G (2020) Paeoniflorin accelerates foot wound healing in diabetic rats though activating the Nrf2 pathway. Acta Histochem 122:151649. https://doi.org/https://doi.org/10.1016/j.acthis.2020.151649
59. Yin M, Wang X, Yu Z, Wang Y, Wang X, Deng M, Zhao D, Ji S, Jia N, Zhang W (2020) γ-PGA hydrogel loaded with cell-free fat extract promotes the healing of diabetic wounds. J Mater Chem B 8:8395–8404. https://doi.org/10.1039/D0TB01190H
60. Nandi S, Sproul EP, Nellenbach K, Erb M, Gaffney L, Freytes DO, Brown AC (2019) Platelet-like particles dynamically stiffen fibrin matrices and improve wound healing outcomes. Biomater Sci 7:669–682. https://doi.org/10.1039/C8BM01201F
61. Han Y, Jiang Y, Li Y, Wang M, Fan T, Liu M, Ke Q, Xu H, Yi Z (2019) An aligned porous electrospun fibrous scaffold with embedded asiatic acid for accelerating diabetic wound healing. J Mater Chem B 7:6125–6138. https://doi.org/10.1039/C9TB01327J
62. Huang X, Li L-D, Lyu G-M, Shen B-Y, Han Y-F, Shi J-L, Teng J-L, Feng L, Si S-Y, Wu J-H, Liu Y-J, Sun L-D (2018) C.-H. Yan, Chitosan-coated cerium oxide nanocubes accelerate cutaneous wound healing by curtailing persistent inflammation. Inorg Chem Front 5:386–393. https://doi.org/10.1039/C7QI00707H
63. Shanmugapriya K, Kang HW (2019) Engineering pharmaceutical nanocarriers for photodynamic therapy on wound healing. Review Mater Sci Eng C 105:110110. https://doi.org/https://doi.org/10.1016/j.msec.2019.110110
64. Milde F, Franco D, Ferrari A, Kurtcuoglu V, Poulikakos D, Koumoutsakos P (2012) Cell Image Velocimetry (CIV): boosting the automated quantification of cell migration in wound healing assays. Integr Biol 4:1437–1447. https://doi.org/10.1039/C2IB20113E
65. Ayal G, Belay A, Kahaliw W (2019) Evaluation of wound healing and anti-inflammatory activity of the leaves of Calpurnia aurea (Ait.) Benth (fabaceae) in mice. Wound Med 25:100151. https://doi.org/https://doi.org/10.1016/j.wndm.2019.100151
66. Xu J, Xu JJ, Lin Q, Jiang L, Zhang D, Li Z, Ma B, Zhang C, Li L, Kai D, Yu H-D, Loh XJ (2020) Lignin-Incorporated Nanogel Serving As an Antioxidant Biomaterial for Wound Healing. ACS Appl Bio Mater. https://doi.org/10.1021/acsabm.0c00858
67. Gao W, Jin W, Li Y, Wan L, Wang C, Lin C, Chen X, Lei B, Mao C (2017) A highly bioactive bone extracellular matrix-biomimetic nanofibrous system with rapid angiogenesis promotes diabetic wound healing. J Mater Chem B 5:7285–7296. https://doi.org/10.1039/C7TB01484H
68. Alipour R, Khorshidi A, Shojaei AF, Mashayekhi F, Moghaddam MJM (2019) Skin wound healing acceleration by Ag nanoparticles embedded in PVA/PVP/Pectin/Mafenide acetate composite

nanofibers. Polym Test 79:106022.
https://doi.org/https://doi.org/10.1016/j.polymertesting.2019.106022

Figures

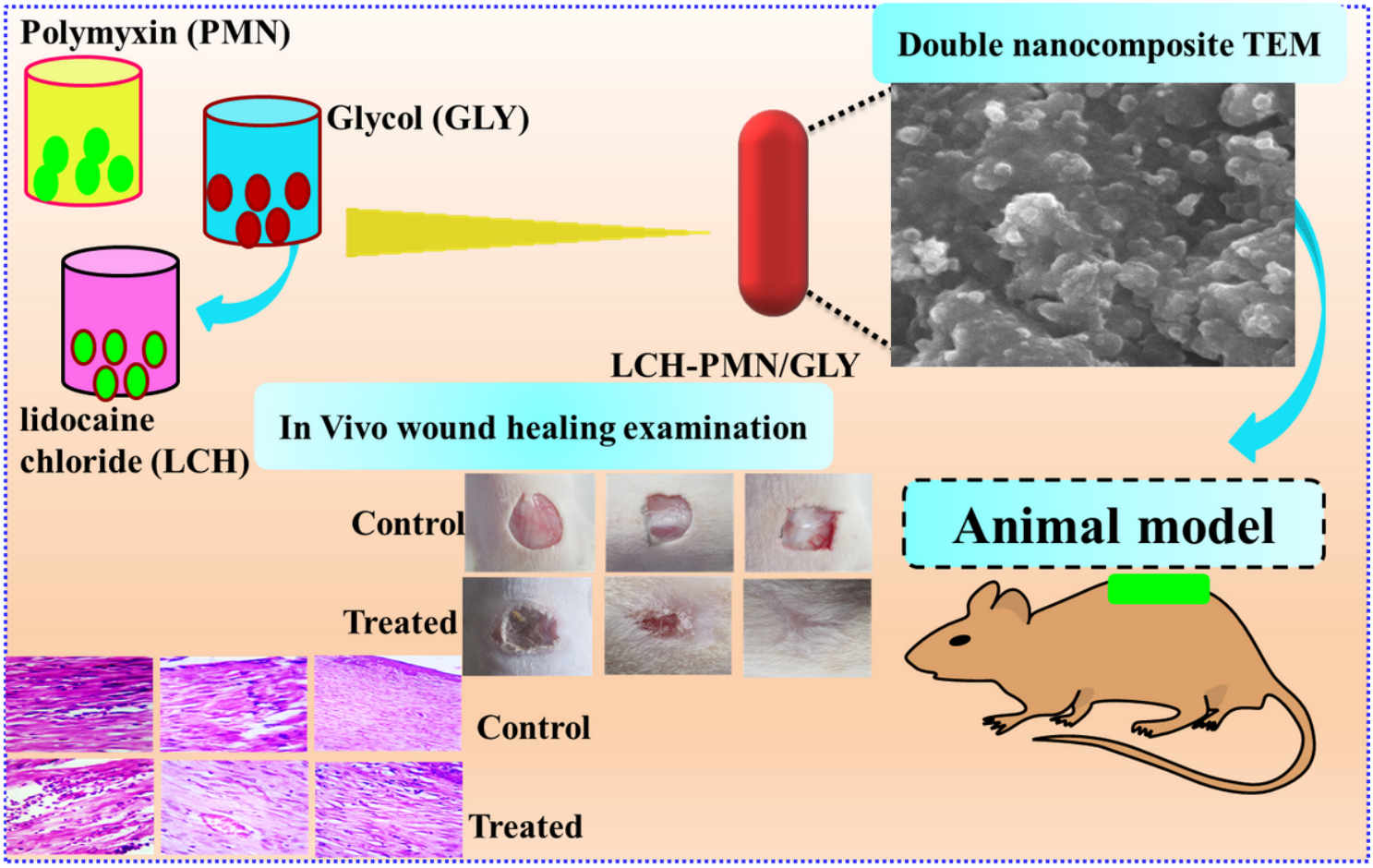

Figure 1

Probable schematic structure of LCH nanocomposite (LCH@PMN/GLY), lidocaine chloride (LCH)-loaded Glycol (GLY)/ Polymyxin B sulphate (PMN). in the wound healing process.

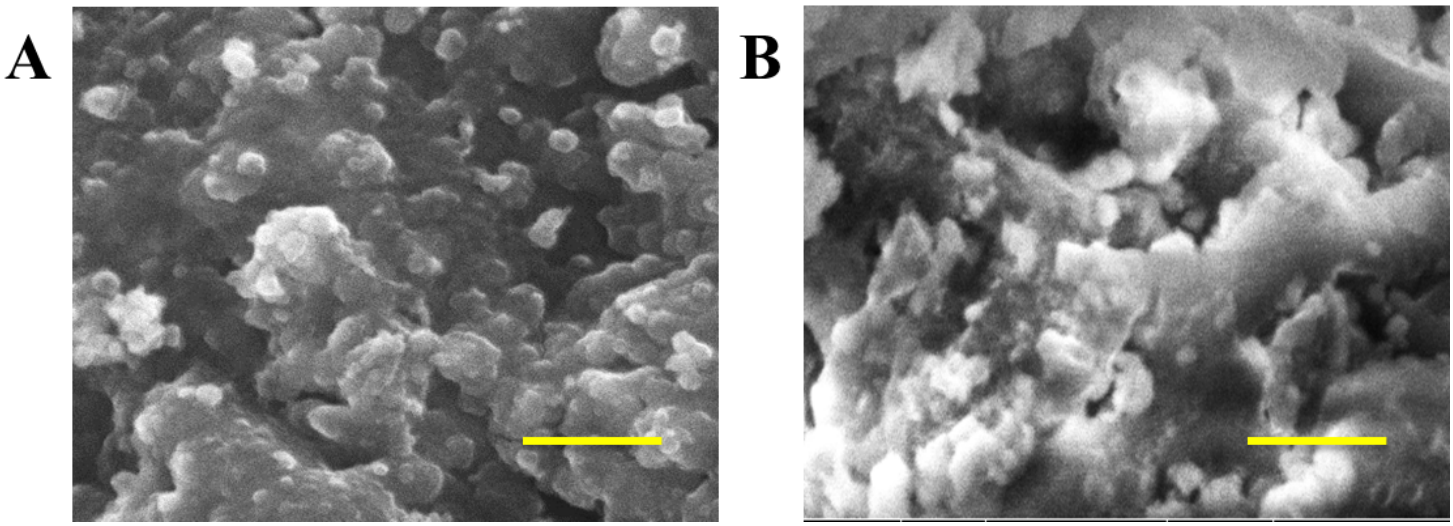

Figure 2

Morphological characterization of developed PMN/GLY and LCH@PMN/GLY. SEM image showing the morphology of (A) PMN/GLY and (B) LCH@PMN/GLY.

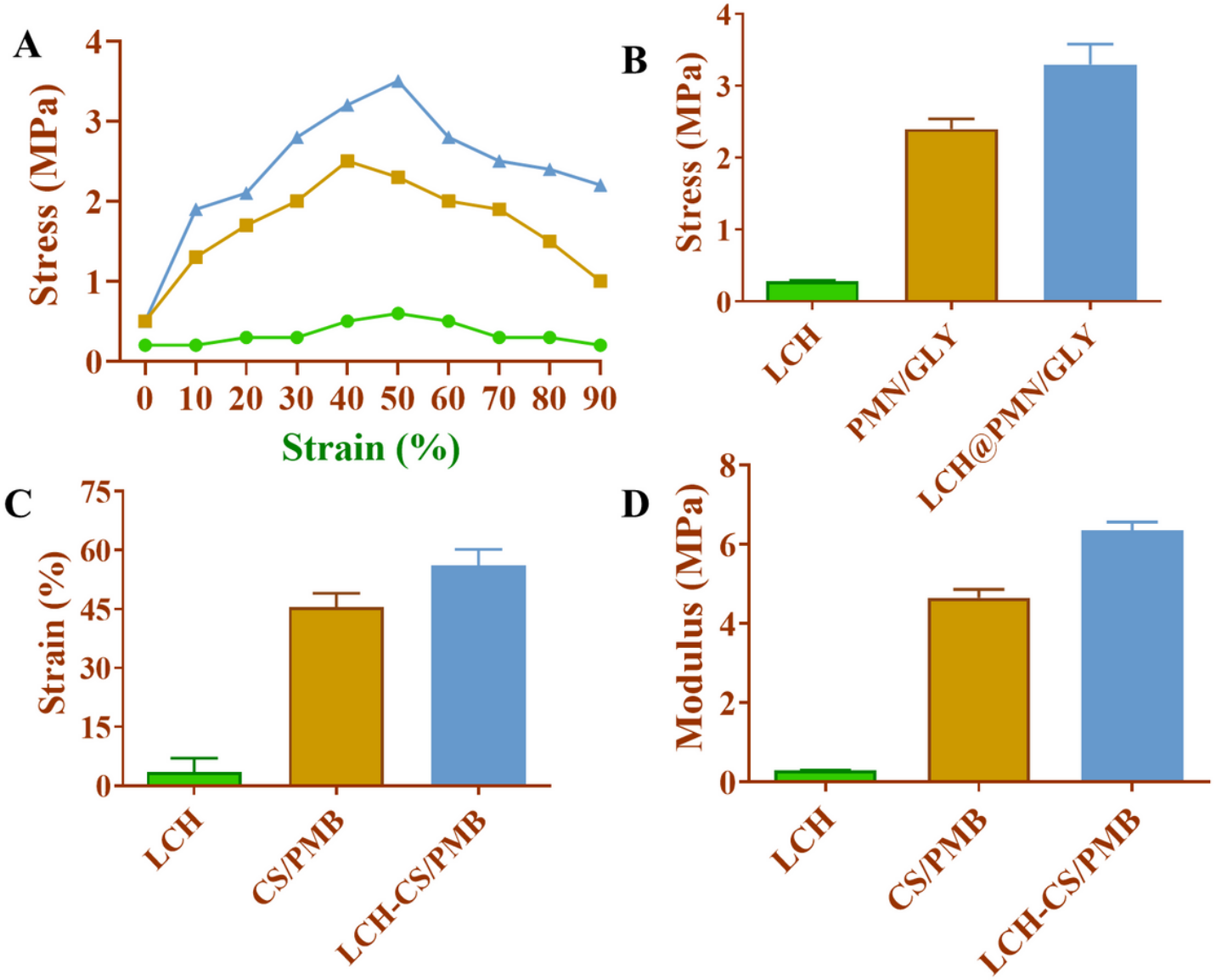

Figure 3

Mechanical properties comparison of A) Stress-strain curve. B) Tensile strength. C) Elongation. D) Tensile modulus of LCH, PMN/GLY and LCH@PMN/GLY nanocomposite.

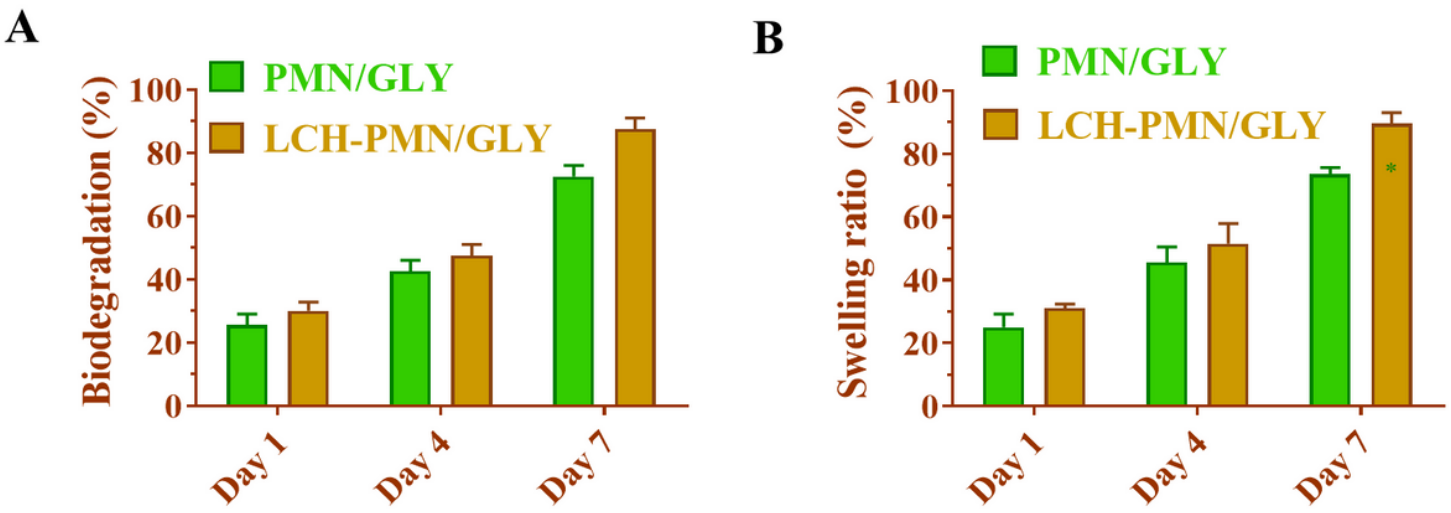

Figure 4

A) Biodegradation and B) Swelling ratio as-fabricated bandages of PMN/GLY and LCH@PMN/GLY nanocomposite using different days (1, 4, and 7) of activity.

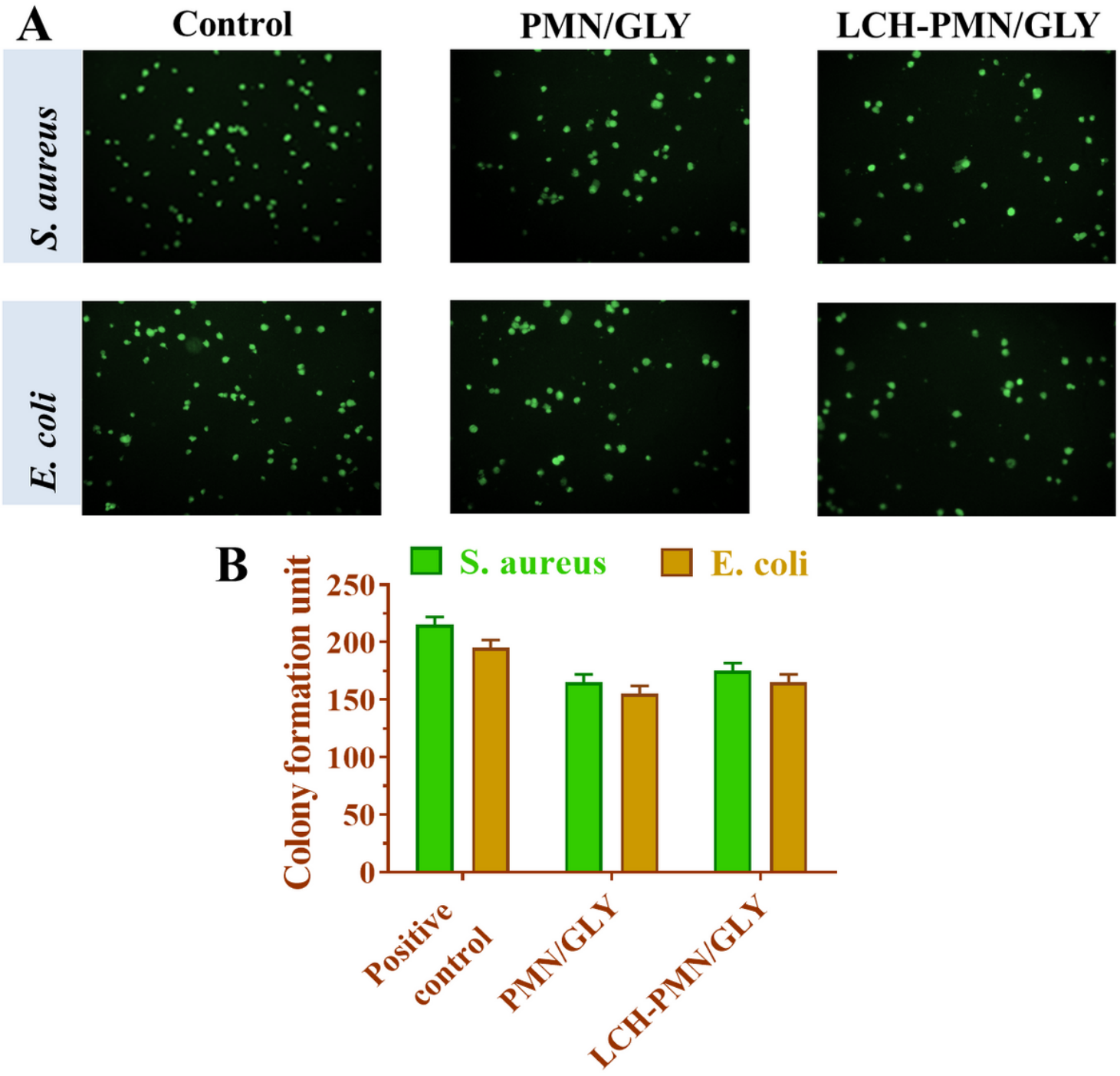

Figure 5

Antibacterial examinations. A) Colony formation of S. aureus and E. coli. B) The bar diagram of respective cell viability of the samples were examined by fluorescence microscopy. The experiments were repeated three times. Values are expressed as the mean ± SD. *p < 0.05, **p < 0.01.

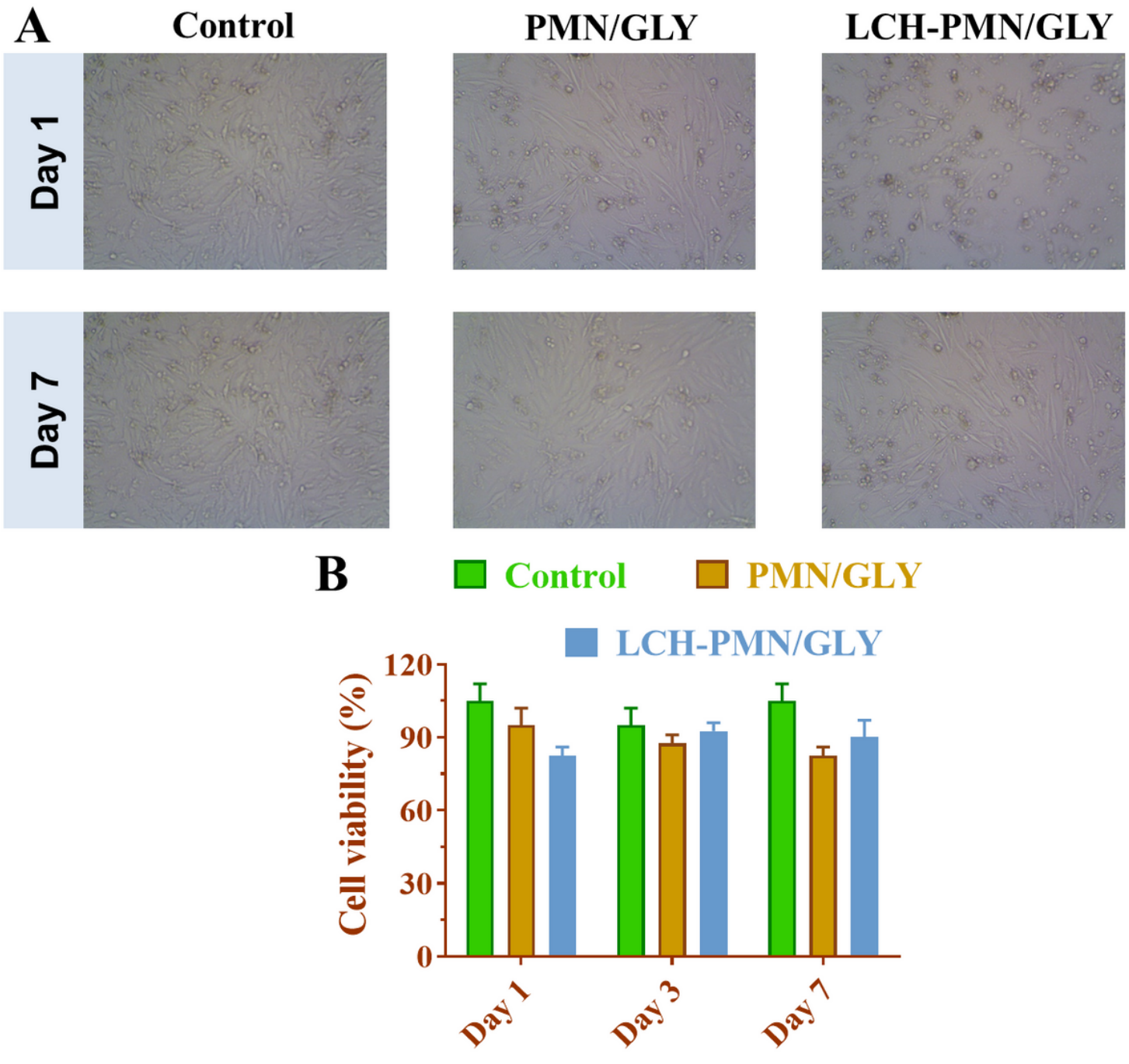

Figure 6

Cell viability examinations. A) Cell viability of PMN/GLY and LCH@PMN/GLY. The experiments were repeated three times. B) The bar diagram of respective cell viability of the samples were examined by fluorescence microscopy. The experiments were repeated three times. Values are expressed as the mean ± SD. *p < 0.05, **p < 0.01.Values are expressed as the mean ± SD. *p < 0.05, **p < 0.01.

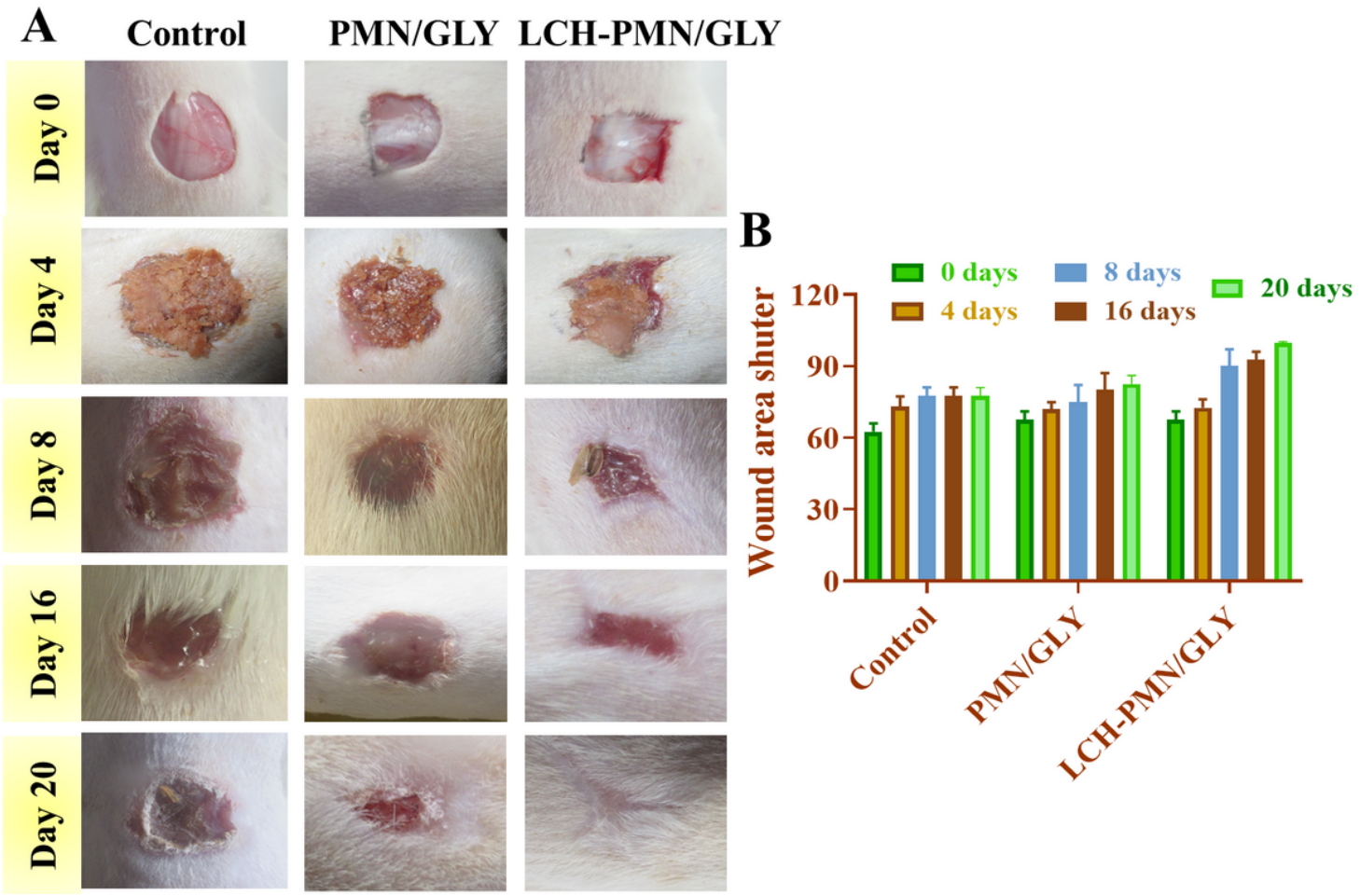

Figure 7

Photographs of an in vivo wound healing study. A) Extent of closure of wounds treated with control, PMN/GLY and LCH@PMN/GLY. B) Evaluation of the wound area shutter. The values are expressed as the mean ± SD. *p < 0.05, **p < 0.01.

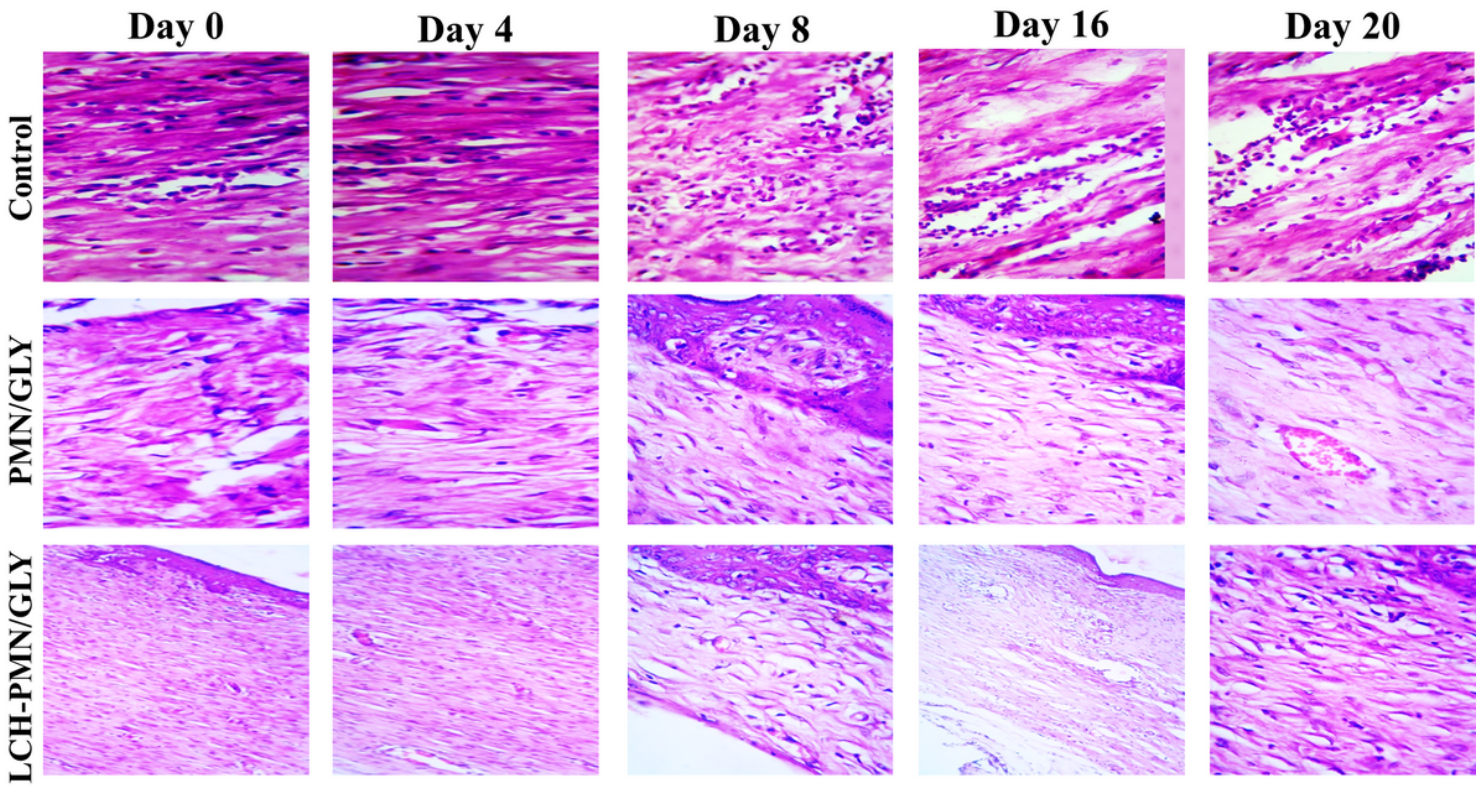

Figure 8

A) Photomicrographs H&E-stained control, as-fabricated bandages of control, PMN/GLY and LCH@PMN/GLY nanocomposite treated wounds.